\



Wideband switchable dual-functional terahertz polarization converter based on vanadium dioxide-assisted metasurface

De-Xian Yan(严德贤), Qin-Yin Feng(封覃银), Zi-Wei Yuan(袁紫微), Miao Meng(孟淼), Xiang-Jun Li(李向军), Guo-Hua Qiu(裘国华), and Ji-Ning Li(李吉宁)

Citation: Chin. Phys. B, 2022, 31 (**1**): 014211. DOI: 10.1088/1674-1056/ac05a7
Journal homepage: http://cpb.iphy.ac.cn; http://iopscience.iop.org/cpb

What follows is a list of articles you may be interested in

Solar energy full-spectrum perfect absorption and efficient photo-thermal generation

Zhefu Liao(廖喆夫), Zhengqi Liu(刘正奇), Qizhao Wu(吴起兆), Xiaoshan Liu(刘晓山), Xuefeng Zhan(詹学峰), Gaorong Zeng(曾高荣), and Guiqiang Liu(刘桂强)

Chin. Phys. B, 2021, 30 (**8**): 084206. DOI: 10.1088/1674-1056/ac0696

Efficient manipulation of terahertz waves by multi-bit coding metasurfaces and further applications of such metasurfaces

Yunping Qi(祁云平) Baohe Zhang(张宝和), Jinghui Ding(丁京徽), Ting Zhang(张婷), Xiangxian Wang(王向贤), and Zao Yi(易早)

Chin. Phys. B, 2021, 30 (**2**): 024211. DOI: 10.1088/1674-1056/abd6fc

Broadband asymmetric transmission for linearly and circularly polarization based on sand-clock structured metamaterial

Tao Fu(傅涛), Xing-Xing Liu(刘兴兴), Guo-Hua Wen(文国华), Tang-You Sun(孙堂友), Gong-Li Xiao(肖功利), and Hai-Ou Li(李海鸥)

Chin. Phys. B, 2021, 30 (**1**): 014201. DOI: 10.1088/1674-1056/abb662

Active metasurfaces for manipulatable terahertz technology

Jing-Yuan Wu(吴静远), Xiao-Feng Xu(徐晓峰), Lian-Fu Wei(韦联福)

Chin. Phys. B, 2020, 29 (**9**): 094202. DOI: 10.1088/1674-1056/aba613

Hyperbolic metamaterials for high-efficiency generation of circularly polarized Airy beams

Lin Chen(陈林), Huihui Li(李会会), Weiming Hao(郝玮鸣), Xiang Yin(殷祥), Jian Wang(王健)

Chin. Phys. B, 2020, 29 (**8**): 084210. DOI: 10.1088/1674-1056/ab96a1

Wideband switchable dual-functional terahertz polarization converter based on vanadium dioxide-assisted metasurface

De-Xian Yan(严德贤)[1,2,4,†], Qin-Yin Feng(封覃银)[1,2], Zi-Wei Yuan(袁紫微)[1,2], Miao Meng(孟淼)[1,2], Xiang-Jun Li(李向军)[1,2], Guo-Hua Qiu(裘国华)[1,2], and Ji-Ning Li(李吉宁)[3]

[1] *Key Laboratory of Electromagnetic Wave Information Technology and Metrology of Zhejiang Province, College of Information Engineering, China Jiliang University, Hangzhou* 310018, *China*
[2] *Center for THz Research, China Jiliang University, Hangzhou* 310018, *China*
[3] *College of Precision Instrument and Optoelectronic Engineering, Tianjin University, Tianjin* 300072, *China*
[4] *State Key Laboratory of Crystal Materials, Shandong University, Jinan* 250100, *China*

(Received 12 April 2021; revised manuscript received 14 May 2021; accepted manuscript online 27 May 2021)

The terahertz technology has attracted considerable attention because of its potential applications in various fields. However, the research of functional devices, including polarization converters, remains a major demand for practical applications. In this work, a reflective dual-functional terahertz metadevice is presented, which combines two different polarization conversions through using a switchable metasurface. Different functions can be achieved because of the insulator-to-metal transition of vanadium dioxide (VO_2). At room temperature, the metadevice can be regarded as a linear-to-linear polarization convertor containing a gold circular split-ring resonator (CSRR), first polyimide (PI) spacer, continuous VO_2 film, second PI spacer, and gold substrate. The converter possesses a polarization conversion ratio higher than 0.9 and a bandwidth ratio of 81% in a range from 0.912 THz to 2.146 THz. When the temperature is above the insulator-to-metal transition temperature (approximately 68 °C) and VO_2 becomes a metal, the metasurface transforms into a wideband linear-to-circular polarization converter composed of the gold CSRR, first PI layer, and continuous VO_2 film. The ellipticity is close to −1, while the axis ratio is lower than 3 dB in a range of 1.07 THz–1.67 THz. The metadevice also achieves a large angle tolerance and large manufacturing tolerance.

Keywords: metasurface, polarization conversion, vanadium dioxide, dual-functional

PACS: 81.05.Xj, 87.50.U–, 42.81.Gs **DOI:** 10.1088/1674-1056/ac05a7

1. Introduction

Terahertz waves in the region between the microwave and infrared frequency regions have high potential applications in future communication networks, such as sixth-generation (6G) systems.[1] The ability to manipulate terahertz waves freely and flexibly has aroused considerable interest in basic and applied studies. In recent years, metasurfaces have attracted increasing attention because of their planar geometries, simple designs, and outstanding controls over the counterparts of electromagnetic fields. Metasurface structures are fundamentally different from traditional optical elements, which are usually curved and spatially extended (*i.e.*, bulky) in shape. Therefore, metasurface-based devices are surface-limited to subwavelength thickness, providing a new route to the realization of very intensive integration and miniaturization in photonics. Numerous attractive applications have been realized through designing the metasurfaces, including surface wave couplers,[2] focusing lenses,[3] optical imaging,[4] broadband absorbers,[5] wave plates,[6] and polarimeters.[7]

The manipulation of the polarization and the transmission characteristics of electromagnetic waves have been demonstrated in microwave,[8] terahertz,[9,10] infrared,[11] and optical[12] frequency regions. Traditional polarization modulation elements including optical gratings[13] and dichroic crystals[14] usually provide narrow operation frequency bands. Wideband characteristics of the reported elements are achieved by stacking various structures with different resonant frequencies[15] or by forming a gradient in the dichroic crystal.[16] However, these designs for wideband responses lead to bulky three-dimensional (3D) devices, which hinders the device from integrating, thereby increasing the complexity, and leading the manufacturing cost to increase.

The interaction of terahertz waves with metasurfaces enables the modulation of the polarization by changing the phase of the incident wave.[17,18] This can be used to construct polarization converters, including linear-to-linear (LTL), linear-to-circular (LTC), and left-to-right or right-to-left circular polarization converters. Most of metasurfaces have been proposed to perform only one function at the operation frequencies, while the freedom and flexibility of metasurface design enable the manufacture of universal polarization converters which is advantageous for device applications with miniaturization and integration. Different types of polarization-manipulated metasurfaces have been designed to provide similar or identical functions. Thus, the effective integration of different functions into a single metasurface has attracted considerable attention,

[†]Corresponding author. E-mail: yandexian1991@163.com
© 2022 Chinese Physical Society and IOP Publishing Ltd

particularly in the terahertz region.

To achieve different functions, the metasurface can be combined with functional materials, such as phase-change materials. Tunable metasurface structures based on different materials (including graphene,[19,20] VO_2,[21] and Dirac semimetals[22]) have been extensively investigated. Among them, VO_2 exhibits a reversible insulator-to-metal (ITM) transition by stimulations of electric, thermal, and optical properties. The conductivity of VO_2 can vary by four or five orders of magnitude during the ITM transition,[23–25] making it a superior choice for the development of tunable terahertz metasurface devices. The phase transition occurs on a time scale of few femtoseconds.[26] Numerous intriguing applications based on VO_2 have been proposed and experimentally investigated for optical devices, including absorbers, modulators, and filters. However, in the terahertz frequency band, the dynamic operation of composite metasurfaces with multi-functional properties has rarely been studied. Therefore, two or more different functions are expected to be integrated into a single metasurface structure.[27,28] For the design of switchable terahertz metasurface devices, Ding *et al.* designed a metasurface combining an absorber and half-wave plate based on the ITM transition of VO_2.[29] Wang *et al.* developed a tunable dual-functional terahertz metasurface structure by using Dirac semimetal films and VO_2.[30] Chen and Song introduced a VO_2 film into a multi-layer structure to realize the two functions of perfect absorption and high transmission through using the ITM phase transition of VO_2.[26] Recently, we reported a single metasurface structure to realize broadband absorption and LTC polarization conversion through using the ITM transition of VO_2.[31] These reported devices with complex structures hinder the metadevices from being designed and fabricated.

In this study, by combining a simple microstructure with the phase transition of VO_2, a dual-functional metadevice is proposed based on a sandwich structure configuration. The proposed metadevice can switch from LTL polarization conversion to another function with LTC polarization conversion by utilizing the ITM phase transition of VO_2. Simulation results indicate that the relative bandwidth of the proposed metadevice used as an LTL converter and LTC converter are approximately 81% and 44%, respectively. This study provides a foundation for the design of switchable multi-functional metadevices in the terahertz frequency band. The structure can also be employed in other frequency regions by changing the structure size.

2. Design of multi-functional metasurface device

Based on the concept of metasurfaces, a 3D schematic diagram of the designed tunable metasurface with different functions operating in the terahertz region based on the ITM transition of VO_2 is shown in Fig. 1. The metasurface consists of different functional layers, including a periodic gold circular split-ring resonator (CSRR), first dielectric layer, continuous VO_2 film, second dielectric layer, and bottom metal substrate.

The metadevice is designed and the corresponding calculation is carried out based on the commercial software CST Microwave Studio. The unit cell boundary conditions are set to be in the x and y directions to simulate infinite arrays, and the open boundaries are added in the z direction. The linearly polarized plane wave travelling in the z direction propagates through the entire structure. As shown in Fig. 1, the parameters of the unit cell are $p_x = p_y = 80$ μm, $t_3 = 10$ μm, $t_2 = 1$ μm, $t_1 = 16$ μm, $R = 30$ μm, $w = 3$ μm, and $\alpha = 15°$. The top metal CSRR layer and bottom substrate are 0.2-μm-thick gold layers each with a conductivity of 4.561×10^7 S/m.[32,33] The top CSRRs are aligned with a clockwise rotation of 45° with respect to the y direction and periodically arranged in the x and y directions. In the simulation, the first and second dielectric layer are of polyimide (PI) with a dielectric constant of $\varepsilon_r = 3.5$ and loss tangent of $\delta = 0.0027$.[34]

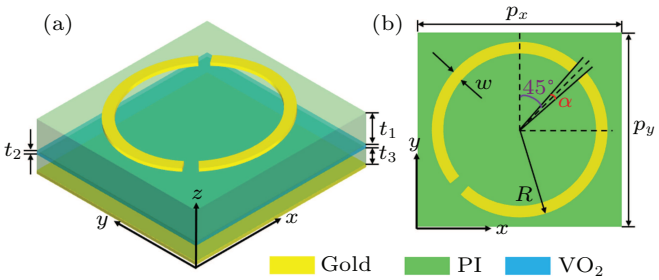


Fig. 1. (a) 3D schematic diagram of design and (b) top view of split-ring resonator.

The continuous VO_2 film of the metasurface can be fabricated by the sol–gel method, which has a lower cost and can be implemented in one process. Different preparation methods can be used, including vacuum evaporation, sputtering, and pulsed laser deposition.[35] Notably, unlike most of terahertz metadevices combined with various materials and complex microstructures, the proposed structure is simple to process, mainly because it contains only the metal CSRRs and continuous VO_2 film, which effectively reduces the complexity of the metadevice.

The ITM transition characteristic of VO_2 in the terahertz region can be determined by the Bruggeman effective medium theory. A detailed description can be found in our previous report.[31] In terahertz frequency band, the dielectric function in the insulating phase is $\varepsilon_D = 9$. And the dielectric function in the metallic phase can be expressed as the Drude model $\varepsilon_M(\omega) = \varepsilon_\infty - \omega_P^2/(\omega^2 + i\omega/\tau)$, where ω is the angular frequency, ε_∞ is the high-frequency limit dielectric constant, $\tau = 2.2$ fs is the carrier collision time, and ω_P is the plasma angular frequency. When VO_2 material is in the insulating phase, then $\varepsilon_\infty = \varepsilon_D = 9$. The VO_2 is modeled as a ma-

terial with a conductivity of $\sigma = -i\varepsilon_0\omega(\varepsilon_C - 1)$ at different temperatures,[36] where ε_C is the dielectric function.[37,38] At room temperature, VO_2 exhibits insulating property in the terahertz frequency region. Thus, the metasurface can be equivalent to an LTL polarization converter including the gold CSRR structure, first PI layer, VO_2 film, second PI layer, and bottom gold substrate. The incident linear terahertz wave can be reflected and converted into a cross-linear terahertz wave. In contrast, when the temperature increases above the phase-transition temperature (approximately 68 °C in the heating process), VO_2 exhibits the ITM transition and only the top part including the top gold CSRR, first PI layer, and VO_2 continuous film operates, which realizes a wideband LTC polarization conversion.

3. Results and discussion

3.1. Reflective LTL polarization conversion

The LTL polarization conversion characteristics of the dual-functional metadevice are verified when VO_2 can be regarded as an insulator at a temperature of 28 °C. The $r_{EE} = |E_{Er}|/|E_{Ei}|$ and $r_{ME} = |E_{Mr}|/|E_{Ei}|$ are defined as the co-(transverse electric (TE)-to-TE, y-to-y) reflection coefficient and the cross-polarization (TE-to-transverse magnetic (TM), y-to-x) reflection coefficient related to the TE-polarized incident field, respectively. The simulated reflection coefficients of the TE-polarized terahertz wave at normal incidence are shown in Fig. 2(a). The cross-polarization reflection coefficient r_{ME} is higher than 0.9 in a frequency range from 0.90 THz to 2.11 THz, while the co-polarized reflection coefficient r_{EE} is lower than 0.3 on average. Thus, an efficient polarization conversion can be achieved by the proposed metasurface structure. The r_{EE} values of the four resonances at $f_1 = 0.984$ THz, $f_2 = 1.362$ THz, $f_3 = 2.012$ THz, and $f_4 = 2.104$ THz reach the local minima of approximately 0.03176, 0.00688, 0.01412, and 0.02242, respectively. The above four resonance points correspond to the high value of r_{ME}. The polarization conversion ratio (PCR) is expressed as $\text{PCR} = r_{ME}^2/(r_{ME}^2 + r_{EE}^2)$ to obtain the efficiency of polarization conversion.[8] Figure 2(a) also shows the simulated PCR as a function of frequency. The PCR of the designed structure is above 0.9 in a range from 0.912 THz to 2.146 THz, which indicates that more than 90% of the incident terahertz TE polarization is converted into cross-polarized (TM polarization) states. In this frequency range, the bandwidth ratio $(f_{max} - f_{min})/[(f_{max} + f_{min})/2]$ is approximately 81%.[39] For the optimized structure, the PCR is higher than 0.9999 at the three resonance frequency points, which achieve the perfect polarization conversion. The wideband performance is provided mainly by the superposition of various resonance modes.[40] The simulated PCR of the designed metadevice as a function of temperature in the heating process is shown in Fig. 2(b). When the temperature increases from room temperature to the heating point temperature of 68 °C the metadevice can be used as an LTL polarization converter and a very high PCR (> 0.9) in a broadband frequency range can be obtained and is accompanied with a slight change. When the temperature is higher than the heating point temperature (around 68 °C), the VO_2 is in the metal phase, so that the wideband LTL polarization conversion disappears. The PCR curve in the cooling condition is also simulated (not shown here). Notably, the PCR does not significantly decrease with the temperature decreasing. This originates mainly from the hysteresis of the ITM transition characteristics of the VO_2 material.[31]

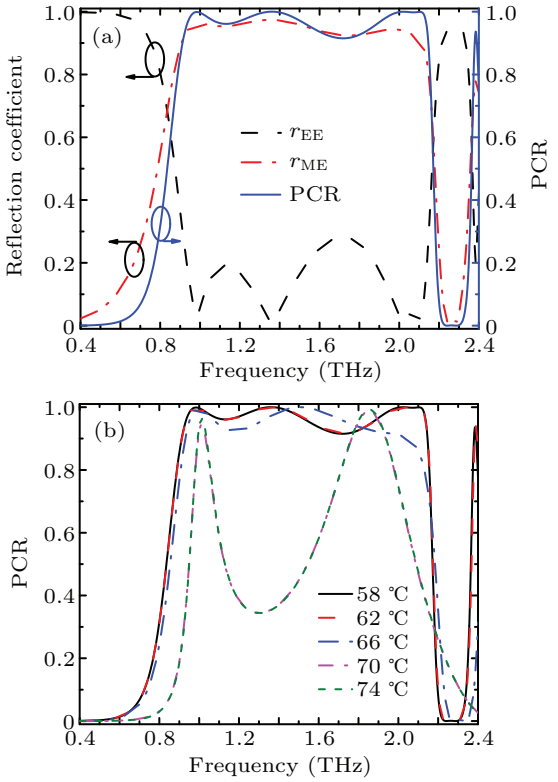


Fig. 2. (a) Frequency-dependent amplitudes of reflection coefficients r_{ME} and r_{EE} and PCR for optimized metasurface structure. (b) Relationships between PCR and frequency at different heating temperatures.

To better investigate the influences of the structural geometry parameters on the polarization conversion performance, the variations of the PCR with geometry parameters (thickness t_3 and width w) are shown in Fig. 3. The resonances of the PCR spectrum are shifted toward lower frequencies with the increase of thickness t_3, *i.e.*, a red-shift appears. In addition, the PCR increases when the frequency region is below the second resonance, but decreases above the second resonance. The size of the CSRR can be changed by adjusting its width w. With the width w increasing from 1 μm to 5 μm, the second resonance shifts toward a lower frequency range, while the first and third resonances are almost unchanged (Fig. 3(b)). Moreover, with t_3 and w changing, the overall bandwidth of the PCR spectrum does not varies significantly.

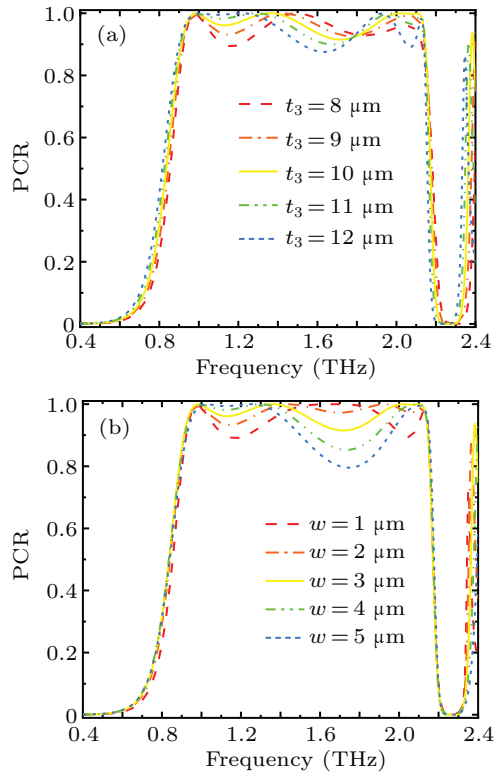


Fig. 3. Simulated variations of PCR with: (a) thickness t_3 and (b) w of metadevice.

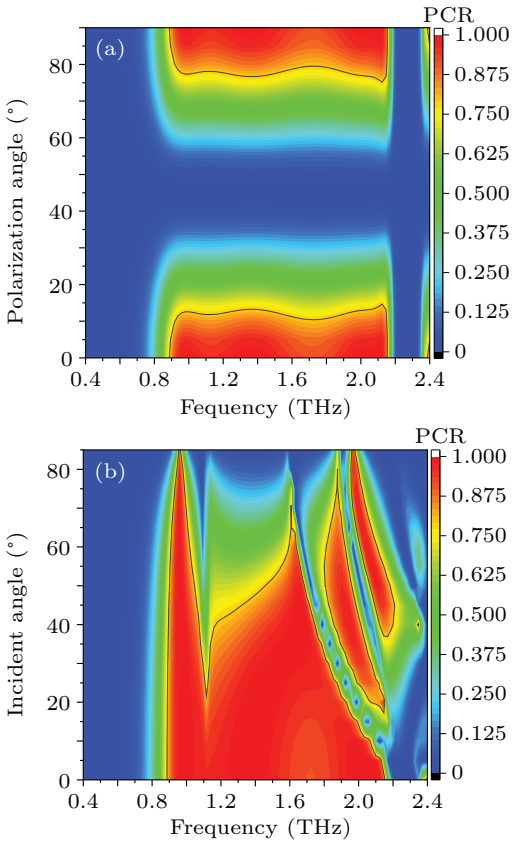


Fig. 4. (a) Simulated frequency-dependent contours of PCR evolving with (a) polarization angle and (b) incident angle for TE polarization.

The variations of the performance of the designed LTL polarization converter with the polarization angle and incident angle are also investigated. Figure 4(a) shows the evolution contour of the PCR when the polarization angle changes from 0° to 90° in steps of 5°. When the polarization angle φ of the incident terahertz wave increases from 0° to 90°, the terahertz wave polarization changes from TE polarization into TM polarization. The results indicate that the structure achieves the same response to the incident terahertz waves with TE polarization as that with TM polarization due to the symmetry properties of the designed metadevice. Figure 4(b) shows the PCR of the TE-polarized terahertz wave as a function of frequency and incident angle θ. During the simulation, θ varies from 0° to 85° in steps of 5°. According to the simulated results, the PCR of the LTL polarization converter is still above 0.8 when θ approaches to 60°. The main PCR peak narrows with the increase of incident angle, while the corresponding PCR remains high at larger incident angles. Some higher-order diffractions appear due to the smaller ratio (1.7) of the operation wavelength (136 μm, 2.2 THz) to the structure period (80 μm).[39]

3.2. Reflective LTC polarization conversion

The above wideband LTL polarization conversion depends on the insulator state of VO_2 at 28 °C. When the temperature is higher than the heating temperature point (approximately 68 °C), VO_2 experiences an ITM transition and becomes metal, providing novel degree of freedom and excellent performance for the control of the polarization state of terahertz waves. Thus, only the top structure consisting of the gold CSRR, first PI layer, and VO_2 continuous film in the metal state operates. In the x–y coordinate system, the co-polarized reflection coefficient r_{EE} and cross-polarized reflection coefficient r_{ME} must be equal, providing a phase difference of $\Delta\varphi = \varphi_{ME} - \varphi_{EE} = 2m\pi \pm \pi/2$ (m is an integer) for the function as an LTC polarization converter, with "−" and "+" denoting the left-circular polarization and the right-circular polarization, respectively.[41] To achieve an efficient polarization conversion in the metasurface structure, the reflection coefficients need to be as large as possible. As shown in Figs. 5(a) and 5(b), when the temperature is approximately 78 °C in a frequency band of 1.07 THz–1.67 THz, the reflection coefficients r_{EE} and r_{ME} exhibit approximately equal intensities. This implies that the TE-polarized incident terahertz wave can be converted into TE and TM polarization component with the same intensity. Furthermore, in the same frequency range, the phase difference $\Delta\varphi$ is approximately 90° for the TE-polarized incident terahertz wave, which is necessary for right circular polarization. The related geometry parameters are $t_3 = 10$ μm, $t_2 = 1$ μm, $t_1 = 16$ μm, $R = 30$ μm, and $w = 3$ μm.

The realization of LTC conversion can be indicated by the ellipticity and axis ratio. The normalized ellipticity of $E = 2|r_{ME}||r_{EE}|\sin(\Delta\varphi)/(|r_{ME}|^2 + |r_{EE}|^2)$ can be defined to estimate the effect of the polarization conversion.[42] An ideal circularly-polarized wave has an ellipticity of 1. When $E =$

-1, the reflected wave is right-circularly polarized. The reflected wave has left-hand circular polarization when $E = +1$. An ellipticity larger than 0.90 is regarded as corresponding to a circularly polarized wave.[43] Figure 5(c) shows the relationship between the ellipticity and terahertz frequency. As shown in Fig. 5(c), the ellipticity is close to -1 in a frequency band of 1.07 THz–1.67 THz, which confirms that the reflective wave is right-hand circularly polarized. The bandwidth ratio is approximately 44%. Notably, when the incident wave is TM-polarized, the reflected wave has circular polarization performances with almost the same bandwidth as but rotating oppositely to the incident wave.

The axis ratio

$$\mathrm{AR} = 10\log_{10}(\tan(0.5 \times \arcsin(2|r_{\mathrm{ME}}||r_{\mathrm{EE}}|\sin(\Delta\varphi)/(|r_{\mathrm{ME}}|^2 + |r_{\mathrm{EE}}|^2))))$$

is also used to evaluate the degree of circular polarization.[44] Figure 5(d) shows the calculated results. The axis ratios of the reflected wave are lower than 3 dB in a wide frequency band of 1.07 THz–1.67 THz, which indicates that the designed metasurface provides a good performance in the LTC polarization conversion.

The energy conversion efficiency can also be expressed as $\eta = |r_{\mathrm{ME}}|^2 + |r_{\mathrm{EE}}|^2$.[41] The efficiency of right circular polarization is higher than 80% at the same frequency (results not shown here). This demonstrates that the designed metasurface possesses the high-efficiency conversion characteristics.

The relationship between the ellipticity and structural parameters (t_1 and w) is studied with normal incidence when the temperature is 78 °C. Figure 6(a) shows the influence of the first PI layer thickness t_1 on ellipticity when the other parameters are unchanged ($t_3 = 10$ μm, $t_2 = 1$ μm, $R = 30$ μm, and $w = 3$ μm). The bandwidth decreases as the thickness t_1 increases from 14 μm to 18 μm. In addition, the intensity increases slightly. The effect of the width w of the gold CSRR on the ellipticity is also investigated. The relations between the ellipticity and the terahertz frequency at different w values are shown in Fig. 6(b) with $t_1 = 16$ μm. As w increases from 1 μm to 5 μm, the bandwidth of ellipticity gradually decreases, while the intensity increases slightly.

Figure 7(a) shows the evolution contour of the axis ratio when the temperature rises from 62 °C to 78 °C As shown in Fig. 7(a), when the temperature is lower than 67 °C the LTC polarization conversion reflection is almost unchanged. However, the LTC polarization conversion reflection decreases rapidly at temperatures higher than 67 °C due to the VO_2 film changing from the insulator to the metal state. The AR of the metasurface varying with incident angle θ and frequency is also investigated, and the results are shown in Fig. 7(b). The designed metasurface can achieve a good circular polarization conversion performance in an ultrabroad band range as θ varies from 0° to approximately 40°. When θ is above 40°, the reflected wave is circularly polarized only in two narrow bands.

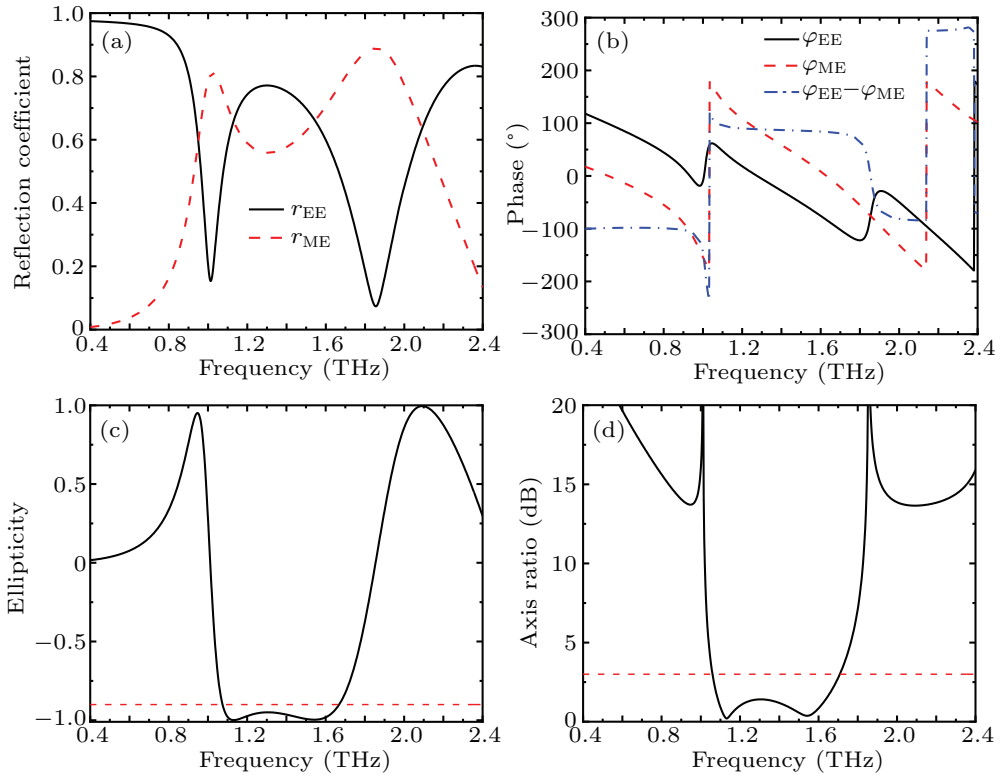


Fig. 5. Stimulated frequency-dependent (a) reflection coefficients, (b) phases for the TE-polarized wave at normal incidence, (c) ellipticity, and (d) axis ratio of metadevice.

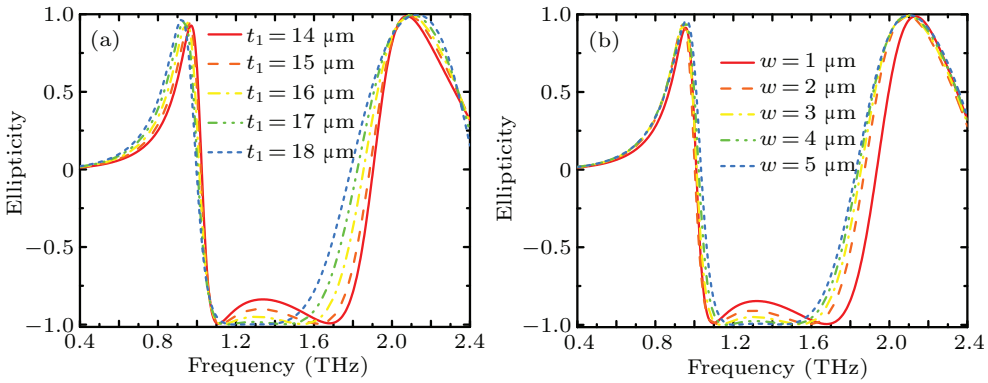


Fig. 6. Relations between ellipticity and frequency at different values of (a) thickness t_1 of the first PI dielectric layer and (b) width w of CSRR.

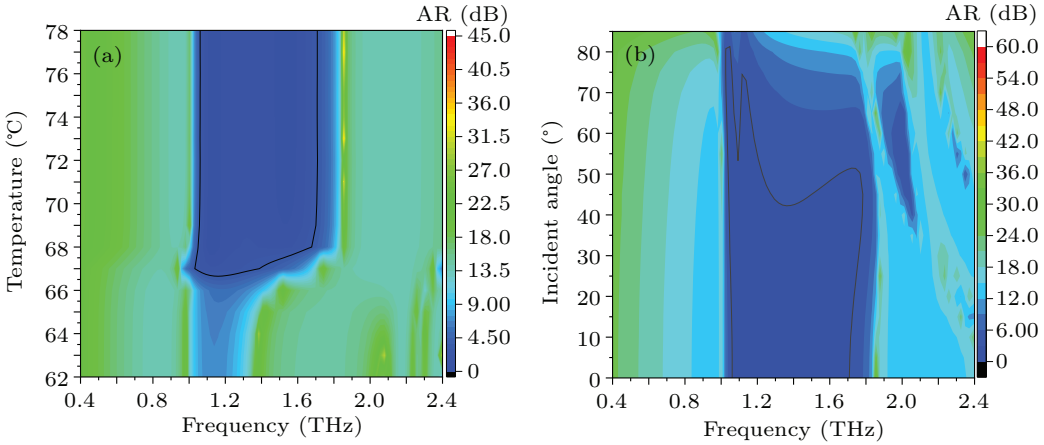


Fig. 7. Simulated frequency-dependent axis ratio varying with (a) heating temperature and with (b) incident angle.

Table 1. Comparisons between proposed device and other devices.

Ref.	Functions	Functional materials	Microstructure	Results
[29]	broadband absorber and HWP	VO_2	two layers microstructure	absorption: absorption > 90% in 0.562 THz–1.232 THz (74.7%); HWP: efficiency exceeding 95% in the bandwidth of 0.49 THz.
[47]	broadband absorber and reflecting surface	VO_2	two layers microstructure	absorber: absorption ~ 97.2% in 0.535 THz–1.3 THz; reflector: reflection > 80% in 0.5 THz– 1.3 THz (88.9%).
[10]	transmission and reflective polarization converter	Dirac semimetals and VO_2	three layers microstructure	transmission: PCR reaches 97.6% at 1.99 THz; reflection: PMR > 88% during 2 THz–3.55 THz (55.9%).
[30]	dual-directional absorber and asymmetric transmission	Dirac semimetal and VO_2	two layers microstructure	absorption: 98.2%; LTL: asymmetric transmission parameter 0.6
[31]	broadband absorption and LTC	VO_2	two layers microstructure	absorber: absorption >90% in 0.74 THz–1.62 THz (74.6%); LTC: ellipticity reaches to −1 in 1.47 Thz–2.27 THz (42.8%).
[48]	LTC	silica+InSb	one layer microstructure	transmission efficiency > 88% with $E < -0.8$ in 0.555 THz–0.737 THz (28.2%).
[49]	LTL	not tunable	three layers microstructure	PCR is near 1 in 0.4 THz–1.1 THz (93.3%).
[43]	LTC	graphene	one layer microstructure	ellipticity: 0.95 in 14 THz–40 THz (96.3%)
This work	LTL and LTC	VO_2	one layer microstructure	LTL: PCR > 0.9 in 0.912 THz–2.146 THz (81%); LTC: ellipticity ~ −1 (AR < 3 dB) in 1.07 THz–1.67 THz (44%)

The recently reported VO_2-based studies provide a practical guidance for our study. The dielectric material PI exhibits stable performances at different temperatures.[35] The fabrication of VO_2-assisted metadevices has been reported.[45,46] A thin VO_2 film is deposited on a PI substrate by using molecular beam epitaxy. Another thick PI layer is then introduced

to the top of the VO_2 film. Subsequently, gold microstructures are fabricated on the top of the PI layer based on traditional lithography and metallization, forming gold CSRRs. The design method presented in this study offers a new approach to the study of multi-functional metasurface-based devices integrating completely different functions into a structure based on the continuous VO_2 film.

The comparisons between the proposed device and previous published devices are conducted as shown in Table 1. Some researches reported dual-functional terahertz metamaterial devices with absorber and polarization converter. Here, by treating the IMT of VO_2 material, we realize the two functions of LTL and LTC in a single metasurface device. Furthermore, compared with the previously reported polarization converters, the proposed device possesses the advantages of efficient linear-to-linear and linear-to-circular polarization conversion through using the single metasurface structure.

The proposed structure has a wide range of practical applications. For example, in broadcast communication with the mid-wave frequency band, linear polarization is usually used to transmit information, while in many cases, circular polarization is generally used in complex climate environments. This is mainly because the circular polarization has the advantage of being easier to adapt to complex electromagnetic environment than linear polarization. The metasurface device can be used to change the polarization of electromagnetic waves to meet the needs of different communication scenarios. In addition, with the rapid progress of high-speed optical communication systems, increasing capacity has become a research hotspot. Orbital angular momentum (OAM) generation is an important application of metasurface and can be widely used in mode division multiplexing of future communication. The OAM generation can be realized by introducing gradient phase discontinuity of the proposed metasurface structure.

4. Conclusions and perspectives

A dual-functional terahertz metadevice with wideband LTL polarization conversion and LTC polarization conversion in a single VO_2-based metasurface structure is proposed. At room temperature, VO_2 is dielectric. The design can be used as a wideband LTL polarization converter under normal incidence in the frequency band of 0.90 THz–2.11 THz. When the temperature increases above 68 °C a wideband LTC polarization converter, converting a TE-polarized wave into a right-hand circularly polarized wave, can be realized. In the frequency band of 1.07 THz–1.67 THz, the ellipticity is almost -1, while the axis ratio is lower than 3. In addition, the wideband and highly efficient dual-functional polarization converter provides a large angle tolerance and large manufacturing tolerance. In this design, the wideband LTL polarization conversion and LTC polarization conversion can be converted into each other based on the ITM transition of VO_2. The designed metadevice has a high potential applications in the fronthaul of terahertz communication and stealth technology.

Acknowledgements

Project supported by the National Natural Science Foundation of China (Grant No. 62001444), the Natural Science Foundation of Zhejiang Province, China (Grant No. LQ20F010009), the Basic Public Welfare Research Project of Zhejiang Province, China (Grant No. LGF19F010003), and the State Key Laboratory of Crystal Materials, Shandong University, China (Grant No. KF1909).

References

[1] Dang S P, Amin O, Shihada B and Alouini M S 2020 *Nat. Electron.* **3** 20
[2] Li X J, Cheng G, Yan D X, Hou X M, Qiu G H, Li J S, Li J N, Guo S H and W. D. Zhou W 2021 *Opt. Lett.* **46** 290
[3] Li X J, Liu Z H, Yan D X, Li J N, Li J S, Qiu G H, Hou X M and Cheng G 2020 *J. Phys. D: Appl. Phys.* **53** 505301
[4] Zang X F, Ding H Z, Intaravanne Y, Chen L, Peng Y, Xie J Y, Ke Q H, Balakin A V, Shkurinov A P, Chen X Z, Zhu Y M and Zhuang S L 2019 *Laser Photon. Rev.* **13** 1900182
[5] Yu P, Besteiro L V, Huang Y. J, Wu J, Fu L, Tan H. K, Jagadish C, Wiederreche G P, Govorov A O and Wang Z M 2019 *Adv. Opt. Mater.* **7** 1800995
[6] Dai L L, Zhang Y P, Guo X H, Zhao Y K, Liu S D and Zhang H Y 2018 *Opt. Mater. Express* **8** 3238
[7] Lin B Q, Lv L T, Guo J X, Wang Z L, Huang S Q and Wang Y W 2020 *Chin. Phys. B* **29** 104205
[8] Li F X, Chen H Y, Zhang L B, Zhou Y, Xie J L, Deng L J and Harris V G 2019 *IEEE T Microw. Theor.* **67** 607
[9] Yang C, Gao Q, Dai L, Zhang Y, Zhang H and Zhang Y 2020 *Opt. Mater. Express* **10** 2289
[10] Wu J Y, Xu X F and Wei L F 2020 *Chin. Phys. B* **29** 094202
[11] Lévesque Q, Makhsiyan M, Bouchon P, Pardo F, Jaeck J, Bardou N, Dupuis C, Haïdar R and Pelouard J 2014 *Appl. Phys. Lett.* **104** 111105
[12] Pfeiffer C, Zhang C, Ray V, Guo L J and Grbic A 2016 *Optica* **3** 427
[13] Liu D and Dai D 2019 *Opt. Express* **27** 20704
[14] Kawai K, Sakamoto M, Noda K, Sasaki T, Kawatsuki N and Ono H 2017 *J. Appl. Phys.* **121** 013102
[15] Jiang Y N, Zhao H P, Wang L, Wang J, Cao W P and Wang Y Y 2019 *Opt. Mater. Express* **9** 2088
[16] Huang Y, Zhou Y and Wu S T 2007 *Opt. Express* **15** 6414
[17] Bu T, Chen K, Liu H, Liu J, Hong Z and Zhuang S 2016 *Photon. Res.* **4** 122
[18] Ding F, Chen Y T and Bozhevolnyi S I 2020 *Photon. Res.* **8** 707
[19] Tang B, Jia Z P, Huang L, Su J B and Jiang C 2020 *IEEE J. Sel. Top. Quantum Electron.* **27** 4700406
[20] Jia Z P, Huang L, Su J B and Tang B 2021 *J. Lightwave Tech.* **39** 1544
[21] Ren Y, Zhou T L, Jiang C and Tang B 2021 *Opt. Express* **29** 7666
[22] Dai L L, Zhang Y P, O'Hara J F and Zhang H Y 2019 *Opt. Express* **27** 35784
[23] Liu H, Lu J and Wang X R 2018 *Nanotechnology* **29** 024002
[24] Lei L, Lou F, Tao K Y, Huang H X, Cheng X and Xu P 2019 *Photon. Res.* **7** 734
[25] Liu W W and Song Z Y 2020 *Carbon* **174** 617
[26] Chen L L and Song Z Y 2020 *Opt. Express* **28** 6565
[27] Wang T L, Zhang Y P, Zhang H Y and Cao M Y 2020 *Opt. Mater. Express* **10** 369
[28] Wang T. L, Zhang H Y Zhang Y P and Cao M Y 2020 *Results Phys.* **19** 103484
[29] Ding F, Zhong S M and Bozhevolnyi S I 2018 *Adv. Opt. Mater.* **6** 1701204
[30] Wang T L, Zhang H Y, Zhang Y, Zhang Y P and Cao M Y 2020 *Opt. Express* **28** 17434

[31] Yan D X, Meng M, Li J S, Li J N and Li X J 2020 *Opt. Express* **28** 29843

[32] Zhang M and Song Z Y 2020 *Opt. Express* **28** 11780

[33] Zhao X, Yuan C, Lv W, Xu S and Yao J 2015 *IEEE Photon. Technol. Lett.* **27** 1321

[34] Li J, Yang Y, Li J N, Zhang Y T, Zhang Z, Zhao H L, Li F Y, Tang T T, Dai H T and Yao J Q 2020 *Adv. Theory Simul.* **3** 1900183

[35] Liu H, Wang Z H, Li L, Fan Y X and Tao Z Y 2019 *Sci. Rep.* **9** 5751

[36] Walther M, Cooke D G, Sherstan C, *et al.* 2007 *Phys. Rev. B* **76** 125408

[37] Choi H S, Ahn J S, Jung J H, *et al.* 1996 *Phys. Rev. B* **54** 4621

[38] Liu H, Fan Y X, Chen H G, Li L and Tao Z Y 2019 *Opt. Commun.* **445** 277

[39] Song Z Y and Zhang J H 2020 *Opt. Express* **28** 12487

[40] Cheng Y Z, Withayachumnankul W, Upadhyay A, Headland D, Nie Y, Gong R Z, Bhaskaran M, Sriram S and Abbott D 2014 *Appl. Phys. Lett.* **105** 181111

[41] Jiang Y N, Wang L, Wang J, Akwuruoha C N and Cao W P 2017 *Opt. Express* **25** 27616

[42] Zi J C, Li Y F, Feng X, Xu Q, Liu H C, Zhang X X, Han J G and Zhang W L 2020 *Phys. Rev. Appl.* **13** 034042

[43] Quader S, Zhang J, Akram M R and Zhu W R 2020 *IEEE J. Select. Top. Quantum Electron.* **26** 4501008

[44] Li Y, Zhang J, Qu S, Wang J, Zheng L, Pang Y, Xu Z and Zhang A 2015 *J. Appl. Phys.* **117** 044501

[45] Zhang C H, Zhou G H, Wu J B, Tang Y H, Wen Q Y, Li S X, Han J G, Jin B B, Chen J and Wu P H 2019 *Phys. Rev. Appl.* **11** 054016

[46] Liu X B, Wang Q, Zhang X Q, Li H, Xu Q, Xu Y H, Chen X Y, Li S X, Liu M, Tian Z, Zhang C H, Zou C W, Han J G and Zhang W L 2019 *Adv. Opt. Mater.* **7** 1900175

[47] Li X, Tang S, Ding F, Zhong S, Yang Y, Jiang T and Zhou J 2019 *Sci. Rep.* **9** 5454

[48] Hou Y Z, Zhang C and Wang C R 2020 *IEEE Access* **8** 140303

[49] Fan J P and Cheng Y Z 2020 *J. Phys. D: Appl. Phys.* **53** 025109